Programming Shape Memory Hydrogel to a Pre-Encoded Static Deformation toward Hierarchical Morphological Information Encryption

Huanhuan Lu, Baoyi Wu,* Xiaoxia Le, Wei Lu, Qiu Yang, Qingquan Liu, Jiawei Zhang,* and Tao Chen*

Morphological information encryption such as gesture and sign language is a traditional but efficient way of information storage and communication. However, due to the limited deformability, almost all of the existing information encryption materials store and deliver information via the pattern or color changes on the 2D plane. Herein, a thermo and ion dual-responsive shape memory hydrogel containing short alkyl chains modified polyvinyl alcohol (PVA-C6) and polyacrylamide-co-polyacrylic acid [P(AAm-co-AAc)], is prepared. In this system, the ion-responsive shape memory process of P(AAm-co-AAc) provides the preprogrammed morphological information and actuating force while the thermo-responsive hydrophobic clusters of PVA-C6 are utilized as a molecular switch to control the deformed posture within the deformation process. Incorporated with a photothermal particle, Fe_3O_4, the photothermal PVA-C6 hydrogel is capable of generating diverse configurations that can be encoded as the corresponding information. With the assistance of the programmable NIR, the hydrogel can transfer to the encoded configuration and decrypt the information. Besides, the obtained morphological information can also be erased by immersing the hydrogel in hot water, in order to avoid the leakage of information. This study motivates the design and fabrication of deformable materials and provides a new insight into the information encrypt materials.

1. Introduction

Information storage and communication is a traditional and indispensable topic in real life. With the shock of information explosion and the concern about information leakage, the demand for information storage materials with high efficiency and safety performance is becoming an urgent problem.[1–3]

Recently, some information that needs to be encrypted could be written or printed on the surface of a 2D substrate via fluorescent inks.[4–7] Thus, the encrypted information was unavailable under natural light but could be decrypted under specific wavelengths of light such as 365 or 254 nm.[8,9] In addition, stimuli-responsive materials, where the stored information could only appear under external stimuli, could also be regarded as an ideal candidate for the encryption of information.[10,11] Despite the aforementioned major achievements, the existing pattern-based information storage materials still face some inevitable problems. For instance, the retention time of the encrypted information (fluorescent pattern) is limited since the decomposition reaction and diffusion of fluorescent molecules.[12,13] Besides, the capacity of the information storage materials is still poor. Therefore, fabricating a novel information storage material with high capacity and safety performance is receiving immense scientific attention.

Gesture is a traditional and common way of communication in a silent scene. The information could be continuously exported via the versatile morphing of hands with the control of the nerve, which cannot be received by non-professionals (**Scheme 1**a). Thus, fabricating morphological information storage materials may be a potential solution. As one of the deformable materials,[14–16] shape memory hydrogels could provide programmable deformations because

H. Lu, B. Wu, X. Le, W. Lu, J. Zhang, T. Chen
Key Laboratory of Marine Materials and Related Technologies
Zhejiang Key Laboratory of Marine Materials and Protective Technologies
Ningbo Institute of Material Technology and Engineering
Chinese Academy of Sciences
Ningbo 315201, P. R. China
E-mail: wubaoyi@nimte.ac.cn; zhangjiawei@tiangong.edu.cn; tao.chen@nimte.ac.cn

The ORCID identification number(s) for the author(s) of this article can be found under https://doi.org/10.1002/adfm.202206912.

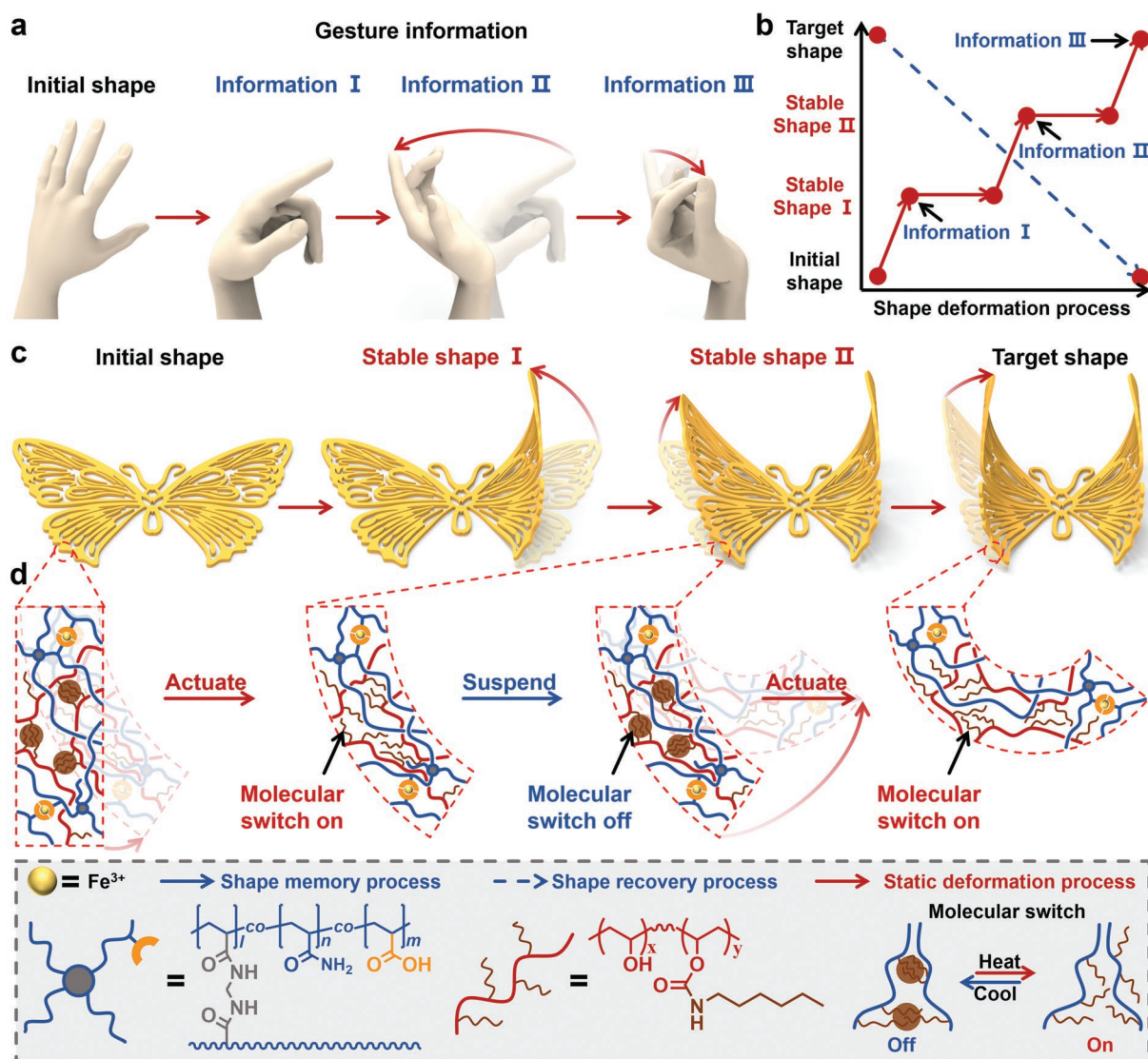**DOI: 10.1002/adfm.202206912**

H. Lu, B. Wu, X. Le, W. Lu, J. Zhang, T. Chen
School of Chemical Sciences
University of Chinese Academy of Sciences
19A Yuquan Road, Beijing 100049, P. R. China

Q. Yang
Ningbo New Material Testing and Evaluation Center Co., Ltd
Ningbo 315000, P. R. China

Q. Liu
Hunan Provincial Key Laboratory of Advanced Materials for New Energy Storage and Conversion
Hunan University of Science and Technology
Xiangtan 411201, P. R. China

Scheme 1. The demonstration and molecular mechanism of gestures-inspired morphological information encryption. a) Schematic illustration showing the gesture information based on the deformation of hands. The different gestures present different information and could be transferred via the deformation of hands. b) Chart showing the morphological information encryption and expression. The different stable shapes represent different information. c) Schematic illustration showing the static deformation process of shape memory hydrogel. The wings of butterfly-shaped hydrogel as first bended by external force and fix the temporary shape in 50 °C FeCl$_3$ solution, then the hydrogel is flattened and fixed in 20 °C. Last, the butterfly-shaped hydrogel could multi-stably self-deform from a flattened shape to a curved shape under the alternate stimulus of heat. d) Schematic illustration showing the static deformation mechanism shape-memory hydrogel. The PVA-C6 is utilized as a molecular switch to control the deformation process via the thermo-responsive hydrophobic clusters.

any pre-coded shape could be fixed via hydrogen bonds, metal-ligand coordination, host-guest interactions, and boronate ester bonds, and provide corresponding deformation under the external stimuli such as pH, heat, and light.[17–19] Although, a few explorations of morphological information storage materials have been implemented,[20,21] the capacity of the encrypted information is still limited for the following reasons: Traditional shape memory hydrogels usually fix the preprogrammed shape which is encoded by external force and generate the shape deformation from a complex temporary shape to a simple original shape (Figure S1, Supporting Information).[22,23] Besides, the key mechanism of shape memory is the generation and

breaking of dynamic temporary crosslinking points. Thus, the shape memory hydrogels with temporary shapes are commonly accompanied by higher crosslinking density and modulus than the original shape. [24,25] This further increases the difficulty of the morphing process from a soft original shape to a tough target shape.

The deformation process of shape deformable hydrogels such as shape memory hydrogels and hydrogel actuators is uncontrollable.[26–28] This means once the deformation process is triggered, it is unpausable. In the past five years, various strategies have been proposed to generate diverse configurations in one hydrogel system by introducing multifunctional

**ADVANCED
SCIENCE NEWS**

www.advancedsciencenews.com

**ADVANCED
FUNCTIONAL
MATERIALS**

www.afm-journal.de

groups or multi-level external stimuli. [29–31]For example, Wu and coworkers fabricated an anisotropic hydrogel containing high-swelling parts and low-swelling parts via multistep photolithography.[32] Due to the asymmetric swelling, the hydrogel could exhibit multi-stable morphs by alternately transferring the hydrogel to different environments. Although the deformations of the existing hydrogels could be elaborately controlled, the number of the configuration is still limited owing to the limited number of external stimuli.

For the above reasons, we aim to incorporate molecular switch into the deformation process to precise and real-time control of the deformation process from the initial shape to target shape and generate plenty of stable intermediate shapes. As shown in Scheme 1b, traditional deformable hydrogel could only exhibit two types of stable morphologies, initial shape, and target shape. Thus, after the morphological information encoding process, there was only one morphological information that could be encrypted or exhibited. On contrary, if the transient shape could be fixed within the deformation process, every transient shape could be encoded as one type of morphology. Moreover, by programmatically regulating two routes of deformation process such as the two sides of a butterfly-shaped hydrogel sheet, the two encoded morphological information could be combined, generating more morphological information (Figure S2, Supporting Information). Therefore, programmatically regulating the static deformation of shape memory hydrogel is an urgent priority.

Herein, we modified the hydrophilic backbone of polyvinyl alcohol with hexylamine (PVA-C6) and applied it to the poly(acrylamide-co-acrylic acid) [P(AAm-co-AAc)] hydrogel network as a molecular switch. As shown in Scheme 1c, based on the thermo-responsive PVA-C6 and ion-responsive P(AAm-co-AAc), the initial butterfly-shaped hydrogel sheet was encoded with the shape information (bended shape) via a two-step shape memory process. When the hydrogel was transferred to hot water, it would bend due to the disassociation of PVA-C6 (switch on). During the deformation process, if the molecular switch was turned off by cooling, the intermediate shape could be immediately fixed via the association of PVA-C6 and the deformation process would be paused (Scheme 1d). Furthermore, when the hydrogel was heated again, the molecular switch would be turned on and the deformation process would restart. Thus, through controlling the molecular switch, three types of configurations could be obtained during the deformation process and the corresponding encoded information could be received and decrypted similar to the transformation of gesture.

Owing to the deformable platform, with the incorporation of photothermal nanoparticles, Fe_3O_4, the photothermal hydrogel was fabricated and the self-deformation could be further remotely controlled by near-infrared light (NIR). With the assistance of programmed NIR, a single photothermal hydrogel strip was able to generate plenty of configurations that could be individually encoded into special information and applied to realize transient information storage. We believe this work would improve the development of shape memory hydrogels toward a new stage of programmable deformation and expand the insight of information storage and encryption materials.

2. Result and Discussion

Thermo-induced crystalline interactions of long alkane chains such as *n*-hexadecane, *n*-octadecane, and *n*-docosane have been proven ideal candidates for shape-memory materials,[24,33] but the hydrophobicity of long alkane chains is too strong to be incorporated into hydrogel with high water content. Thus, the short alkyl chains (hexylamine) were modified to the side of hydrophilic backbone (polyvinyl alcohol, PVA), and denoted as PVA-C6, where the C6 stands for the number of carbon atoms in the side chains (Figure S3, Supporting Information). In order to quantitatively measure the modification ratio of short alkyl, the PVA-C6 was dissolved in d_6-DMSO and analyzed by ^1H NMR. As shown in Figure S4 (Supporting Information), there was a characteristic peak in chemical shift of 6.45, which represented the H of -NH- and proved that the hexylamine was successfully modified to the backbone of PVA. According to the integral area ratio of the ^1H NMR spectrum, the modification rate of PVA-C6 is ≈45%.

Due to the hydrophobicity of short alkyl side chains, the PVA-C6 powder could not be dissolved by water. So, the PVA-C6 power was dissolved by dimethyl sulfoxide (DMSO) and further prepared hydrogel precursor contained acrylamide (AAm) and acrylic acid (AAc) as monomers, *N*, *N'*-methylene bis(acrylamide) (BIS) as crosslinker and ammonium persulphate (APS) as initiator. After polymerization and solvent exchange by water, the PVA-C6 hydrogel was obtained (**Figure 1**a). As shown in Figure 1b, the as-prepared PVA-C6 organogel with DMSO as filler is transparent, and the transmittance is over 60% under the light wavelength from 400 to 800 nm, while the PVA-C6 hydrogel with water as filler is opaque, the transmittance is almost zero because of the microphase separation of short alkyl chains in water. Besides, benefiting from the association of short side alkyl chains, the mechanical property of PVA-C6 hydrogel would be enhanced by almost one order of magnitude. In detail, when one side of the as-prepared PVA-C6 hydrogel strip was clamped, the hydrogel strip would droop due to the soft property with a strain of 390% and stress of 120 kPa. However, after the solvent exchange, the PVA-C hydrogel would not droop and become tougher with a strain of 412% and stress of 931 kPa (Figure 1c).

There were two types of crosslinking interactions in the network of PVA-C6 hydrogel, the stable chemical crosslinking interactions caused by the covalent bonds and plenty of dynamic physical crosslinking interactions caused by the hydrophobic association of short side alkyl chains. Due to the thermo-responsive property of short-side alkyl chains, when the hydrogel was immersed in 60 °C water, these hydrophobic clusters would disassociate. In contrasted, when the hydrogel was immersed in 25 °C water, the hydrophobic clusters would reform, which induced the reversible mechanical property (Figure S5 and Movie S1, Supporting Information). Moreover, the thermo-triggered association and disassociation could also be proved by SEM images, where the pore size of PVA-C6 at 25 °C is smaller than the pore size at 60 °C (Figure S6, Supporting Information). Although a lot of works have reported and proved the thermo-induced crystallization property of PVA chains, the thermo-responsive property of PVA-C6 hydrogel is major credited to the association of short
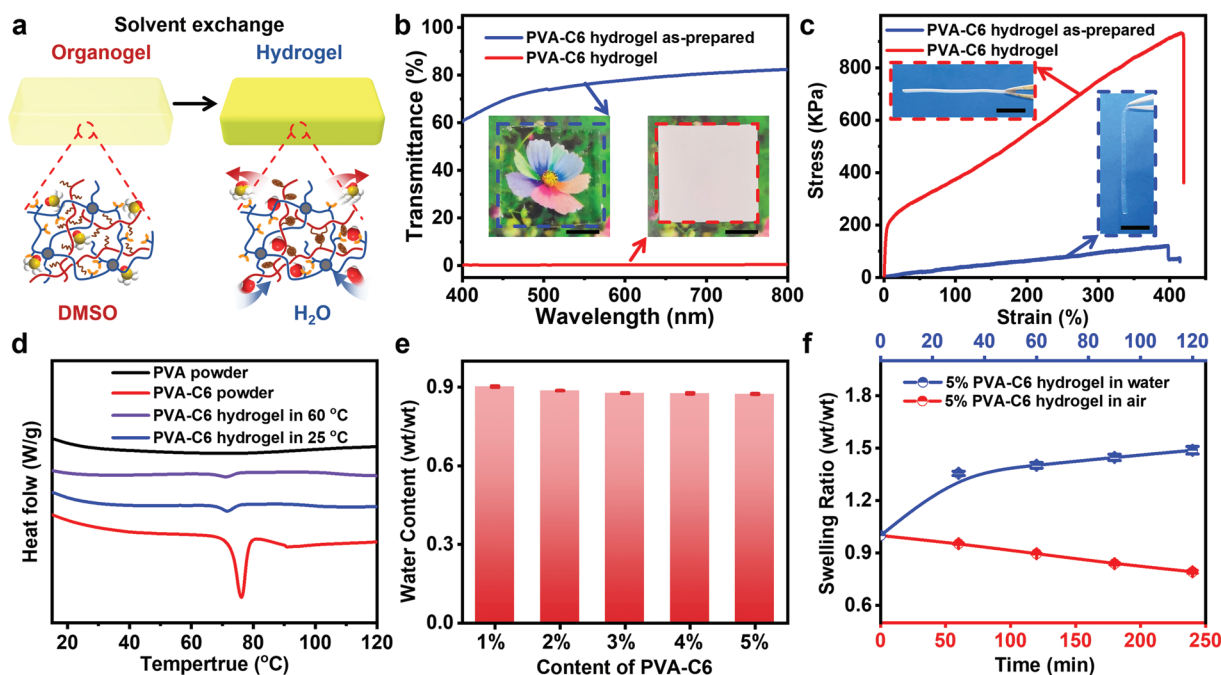
ADVANCED
SCIENCE NEWS
www.advancedsciencenews.com

ADVANCED
FUNCTIONAL
MATERIALS
www.afm-journal.de

Figure 1. The intrinsic performance of PVA-C6 hydrogel. a) Schematic illustration showing the solvent exchange process of PVA-C6 hydrogel. b) The transmittance of PVA-C6 hydrogel before and after solvent exchange. c) The Stress-strain curves of PVA-C6 hydrogel before and after solvent exchange. d) DSC curves of PVA powder (black line), PVA-C6 powder (red line), PVA-C6 hydrogel in 60 °C (purple line), and PVA-C6 hydrogel in 25 °C (blue line). e) The water content of PVA-C6 hydrogels with different content of PVA-C6. f) The anti-swelling and anti-water loss properties of PVA-C6 hydrogel with different content of PVA-C6. Scale bars : 1 cm.

side alkyl chains. Therefore, DSC is utilized for the thermal analysis of PVA powder, PVA-C6 powder, PVA-C6 hydrogel in 25 °C, and PVA-C6 hydrogel in 60 °C. As shown in Figure 1d, there is no obvious peak in the DSC curve of PVA powder while a peak of PVA-C6 powder at 75 °C, which indicated that the major factor responsible for the thermo-responsive mechanics is identified as the association of short side alkyl chains. It is worth to be noted that even though the PVA-C6 powder is introduced into the hydrogel network of P(AAm-co-AAc), the thermo-responsive mechanics are still existing but the temperature and intensity of the peak in the DSC curve will decrease for the low content of PVA-C6. Besides, the weak peak in the DSC curve of PVA-C6 hydrogel in 60 °C indicated that the hydrophobic clusters would not disassociate completely even in 60 °C water.

It is well known that the introduction of hydrophobic additives would destroy the hydrophilic system of the hydrogel. And the existed feasible solution is decreasing the water content of hydrogel or fabricating organogel/organohydrogels. However, in our system, the excellent thermo-responsive association of PVA-C6 powder endows the PVA-C6 hydrogel with efficiently thermal mechanic properties even in the case of the lower content of additives. In addition, the hydrophilic property of PVA backbone and P(AAm-co-AAc) furtherly maintain the hydrophilic system of hydrogel. Therefore, although the water content of the PVA-C6 hydrogel will decrease with the increasing content of PVA-C6, the average water content is still able to reach 90% (Figure 1e). This indicated the PVA-C6 hydrogel can be regarded as a hydrogel, not organohydrogel. Moreover, the addition of PVA-C6 could also increase the anti-swelling and

anti-water loss properties of PVA-C6 hydrogel since the hydrophobic clusters and tough network are able to counteract the swelling of hydrophilic network and the evaporation of water (Figure S7, Supporting Information). As shown in Figure 1f, when the PVA-C6 hydrogel was immersed in water, the swelling ratio will quickly increase to 1.4 and keep constant while the ordinary P(AAm-co-AAc) hydrogel will swell ten times the weight or even break the network. Similarly, when the PVA-C6 hydrogel was exposed to the air, the hydrogel could still maintain 80% water within 250 min while the ordinary hydrogel would lose water quickly. The excellent environmental stability of PVA-C6 hydrogel motivated us to explore its further function and application of it.

The thermo-induced association of PVA-C6 powder not only endows the PVA-C6 hydrogel with thermal mechanic property but also the thermo-responsive shape memory property. According to the dynamic oscillatory frequency sweeps of PVA-C6 hydrogel, the modulus of PVA-C6 hydrogel at 20 °C is higher than that of it at 50 °C since the hydrophobic clusters of short side alkyl chains would associate with lower temperature while disassociating in higher temperature. Moreover, with the increased content of PVA-C6, the modulus gap of PVA-C6 between 20 °C and 50 °C would increase, which indicates that the shape memory property would increase too (Figure S8, Supporting Information). In order to quantitatively analyze the shape memory ability, the PVA-C6 hydrogel strip was bended into a circle by the external force in 50 °C water first, then the hydrogel circle was immersed in the 20 °C water and the temporary shape was fixed via the thermo-induced association of PVA-C6. At last, the shape memorized hydrogel could recover

to the initial shape at 50 °C. As shown in Figure S9 (Supporting Information), when there is low content of PVA-C6 in PVA-C6 hydrogel, the temporary shape is hard to be fixed and the corresponding shape fixity ratio is only 20%. Whereas, with the increase of the content of PVA-C6, more and more hydrophobic clusters would be generated and applied as a temporary crosslinking point to fix the temporary shape, which increases the shape fixity ratio to 80%. In addition, the shape recovery ratio is generally higher than the shape fixity ratio because of the stable chemical network of P(AAm-co-AAc).

Similarly, due to the P(AAm-co-AAc) network, the PVA-C6 hydrogel could also exhibit ion-responsive shape memory property via the metal-ligand coordination, which could also provide a modulus gap before and after the coordination (Figure S10, Supporting Information). During the ion-responsive shape memory process, the PVA-C6 hydrogel strip was bended as before and immersed in 0.1 M $FeCl_3$ solution for 30 s. Thus, the deformed shape was fixed via the metal-ligand coordination between Fe^{3+} and carboxyl groups of P(AAm-co-AAc), and the hydrogel would recover to the initial shape after the metal-ligand coordination was broken by ethylene diamine tetraacetic acid (EDTA). Compared with the thermo-responsive shape memory process, the major influence factor of shape fixity ratio is not the content of PVA-C6 but the treatment time. As shown in Figure S11 (Supporting Information), with the increase of PVA-C6 content, there is no difference in the ion-responsive shape fixity ratio. But when the treatment

time increases from 15 s to 75 s, the shape fixity ratio would increases from 60% to 80% (Figure S12, Supporting Information). Although the thermo and ion have been regarded and proven as non-interfering interactions, the factor of thermo still plays a minor role in the process of ion-responsive shape memory. For example, in our system, when the treatment time of Fe^{3+} is long enough (> 60 s), there is no difference in ion-responsive shape fixity ratio in 20 °C water or 50 °C. But, if the treatment is short, the ion-responsive shape fixity ratio of 50 °C is better than that of 20 °C. Because the network of PVA-C6 would become softer at 50 °C due to the dissociation of short side alkyl chains, which improved the efficiency of diffusion and coordination of Fe^{3+} (Figure S13, Supporting Information).

Based on the discussion above, the morphological information could be encoded into the hydrogel via the first shape memory process and encrypted via the second shape memory process in theory. As shown in **Figure 2**a, the PVA-C6 hydrogel strip was deformed into an "S" shape by external force in 50 °C water, then the hydrogel was immersed into the solution of $FeCl_3$ to fix the temporary shape I (morphological information), the shape fixity ratio is denoted as R_{f1}. Subsequently, the "S" shaped hydrogel was flattened to the initial shape and transformed to 20 °C water in order to fix the temporary II (encrypted morphological information), the corresponding shape fixity ratio is denoted as R_{f2}. At last, the hydrogel strip, temporary II, could self-deform to the "S" shape in the 50 °C water and the shape recovery ratio is denoted as R_r (Figure 2b).
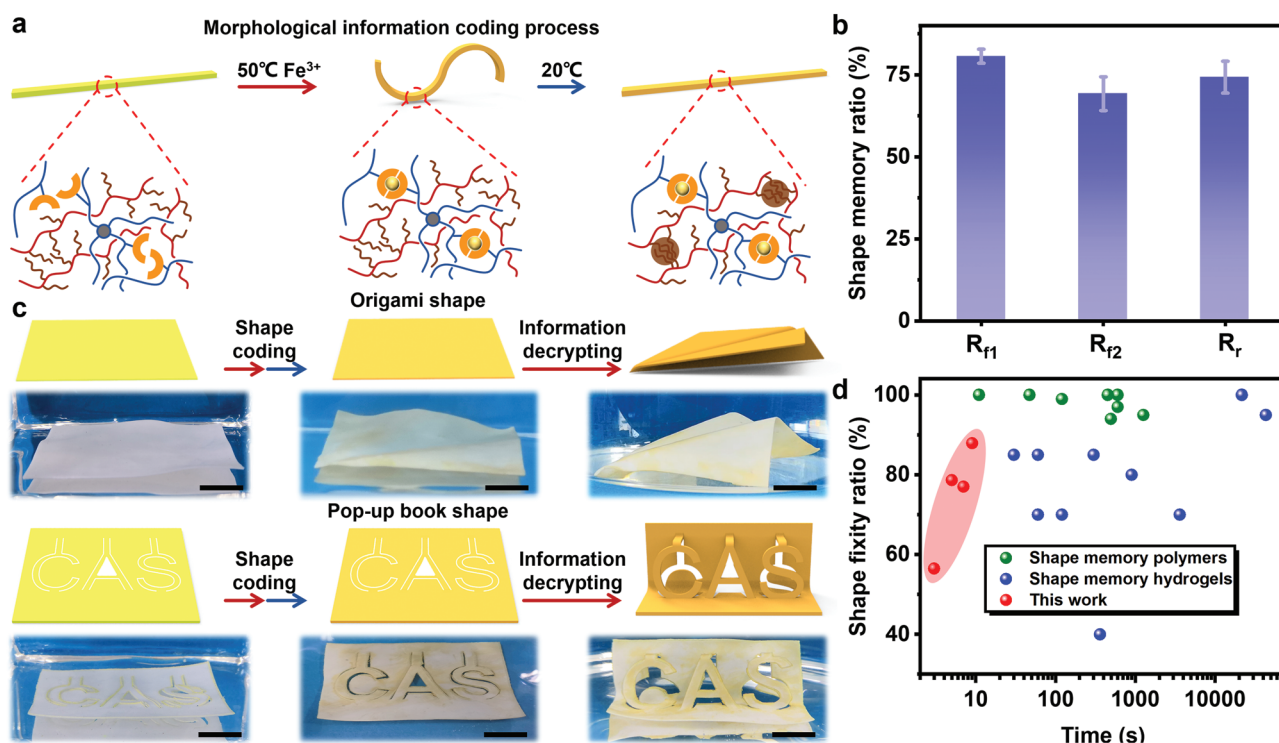

Figure 2. The morphological information coding process and shape memory property of PVA-C6 hydrogels. a) Schematic illustration showing the morphological information coding process. The hydrogel strip was bended into an "S" shape and fixed the temporary shape in 50 °C Fe^{3+} solution first. Then the hydrogel strip was flattened in 50 °C and fixed the temporary shape in 20 °C. b) The thermo and ion dual-responsive shape fixity ratio and shape recovery ratio of PVA-C6 hydrogels. c) Schematic illustration and images showing the information decryption process of PVA-C6 hydrogel via programmable deformation. d) Comparison of shape fixity ratio of shape memory materials including shape memory polymers[25,34–40] and shape memory hydrogels[9,22,23,41–47]. Scale bars : 1 cm.

ADVANCED
SCIENCE NEWS
www.advancedsciencenews.com

ADVANCED
FUNCTIONAL
MATERIALS
www.afm-journal.de

According to the influencing factors of thermo and ion dual-responsive shape memory, the R_{f1}, R_{f2}, and R_r are balanced to 80%, 70%, and 75% respectively in order to ensure the integrity of the whole process (Figure S14, Supporting Information). Besides, the hydrogel strips could also be encoded other morphological information such as "V" or "Ω" shapes in the same way and decrypted the information via the self-deformation in hot water (Figure S15, Supporting Information). Based on the shape coding process, more types of morphological information could be encoded and encrypted. For example, inspired by origami, a 2D PVA-C6 hydrogel sheet could be folded into the 3D airplane shape due to its excellent mechanical property. Then, the temporary shape I was fixed in 50 °C FeCl$_3$ solutions. After flattening and immersing into 20 °C water, the hydrogel sheet that had been encoded with the information of 3D airplane shape was obtained. And the hydrogel sheet was able to self-deform to a 3D airplane shape when triggered by heat again (Figure 2c). Furtherly, when the hydrogel sheet was pre-engraved by laser cutter and incorporated with origami, the hydrogel sheet could self-deform into a 3D pop-up book with the information of the English letter "CAS" after the twice shape memory process, while the traditional deformation process could only deform from 3D target shape to the 2D initial shape (Figure 2d).

As mentioned above, the hydrophobic clusters of short-side alkyl chains not only endow the PVA-C6 hydrogel with excellent mechanical properties of bendable and foldable but also endow it with efficient thermo-induced shape memory property of high shape fixity ratio and fast response. Compared with traditional shape memory materials including shape memory hydrogels and shape memory polymers, the thermo-responsive PVA-C6 hydrogel is able to fix the temporary shape with a shape fixity ratio of 56% in 3 s or a shape fixity ratio of 80% in 9 s (Figure 2e; Movie S2, Supporting Information). The shape memory property of the PVA-C6 hydrogel with 90% water content, far exceeds that of traditional shape memory hydrogels and is comparable to bulk shape memory polymers. Therefore, the hydrophobic clusters of short-side alkyl chains will play a more and more important role in the dynamic crosslinking interactions of shape memory hydrogels.

Subsequently, in order to expand the functions of the PVA-C6 hydrogel, Fe$_3$O$_4$ nanoparticles (Fe$_3$O$_4$ NPs) were introduced into the network to fabricate the PVA-C6 photothermal hydrogel with remote-controllable deformation property. Benefiting from the photothermal effect of Fe$_3$O$_4$ NPs, the PVA-C6 photothermal hydrogel would be heated under near-infrared light (NIR, 808 nm) (**Figure 3**a). As shown in Figure 3b, when the PVA-C6 photothermal hydrogel was exposed to NIR (5 W), the temperature of the hydrogel could quickly rise to 50 °C in 60 s and the maximum temperature could reach 57 °C under water. In contrast, when the NIR was removed, the temperature would quickly decrease to room temperature with the assistance of heat conduction of water. Thus, based on the excellent photothermal effect, the PVA-C6 photothermal hydrogel exhibits remote-controllable and multi-stable deformation properties. For example, a PVA-C6 photothermal hydrogel strip was bended into a circle and fixed the temporary shape in 20 °C water first, then the NIR irradiated continuously to the hydrogel which induced the shape recovery process and the hydrogel strip would deform from 318 ° to 156 ° in 108 s (Figure 3c). Moreover, when the NIR irradiated intermittently to the hydrogel, the PVA-C6 photothermal hydrogel could furtherly exhibit multi-stable deformation. For instance, when the NIR irradiated to the circular PVA-C6 photothermal hydrogel, the hydrogel would deform from 330 ° to 281 ° in 20 s. Then turn off the NIR, with the quick decrease of temperature, the transient shape would be quickly fixed via the association of short side alkyl chains. After 20 s, turn on the NIR again, the shape recovery process would be rebooted and the hydrogel deformed from 278 ° to 243 ° due to the combination of photothermal effect of Fe$_3$O$_4$ NPs and thermo-induced shape memory property of PVA-C6 (Figure S16, Supporting Information). It is worth noting that when the NIR was turned off, the shape recovery process would still continue for a short time due to the residual temperature of the hydrogel.

Furthermore, a PVA-C6 photothermal hydrogel strip was folded and shape memorized, when the NIR locally irradiated to the deformed area, the width of the folded hydrogel would increase while the height would decrease (Figure 3d; Movie S3, Supporting Information). Similar to the multi-stable deformation mentioned above, the folded hydrogel strip could also exhibit continuous multi-stable deformation during the shape recovery process under intermittent NIR (Figure 3e; Movie S4, Supporting Information). In order to quantitatively analyze the innovative deformation process, the characteristic shape parameter (RSP) which was defined as the ratio between the height and width of the folded shape, was applied to describe the state of deformation. As shown in Figure 3f, the value of RSP quickly decreases with the irradiation of NIR and stops in a platform when the NIR is turned off, which indicates the folded hydrogel strip deforms to the stable shape I and keeps the state. Then when the NIR was turned on again, the folded hydrogel strip would furtherly deform to the stable shape II, III, and IV respectively and the corresponding platform can be observed on the curve of RSP.

In addition, a butterfly-shaped PVA-C6 photothermal hydrogel sheet could also be encoded into the wings spread shape in the same way. In the traditional condition, the butterfly-shaped hydrogel sheet with wings spread shape would directly deform to the flattened butterfly shape triggered by heat or NIR, which means the deformation process was single and uncontrollable. However, in our multi-stable deformation system, the left wing of the butterfly-shaped hydrogel would gradually flatten first when a NIR locally irradiated on the left wing. When the irradiation area transfers to the right wing, the right wing of the butterfly-shaped hydrogel would gradually flatten. Therefore, the butterfly-shaped hydrogel could provide four stable states during the deformation process from wing spread shape to wing flatten shape (Figure 3g, Movie S5, Supporting Information). Overall, the excellent photothermal effect of PVA-C6 photothermal hydrogel made the deformation process more controllable, which means the hydrogel could be precisely controlled to an expected shape during the deformation process by the programmable irradiation of NIR.

As mentioned above, traditional shape memory hydrogels could only provide unidirectional shape deformation, from the target shape to the initial shape, but the dual-responsive hydrogels could provide reversible shape deformation, from the initial
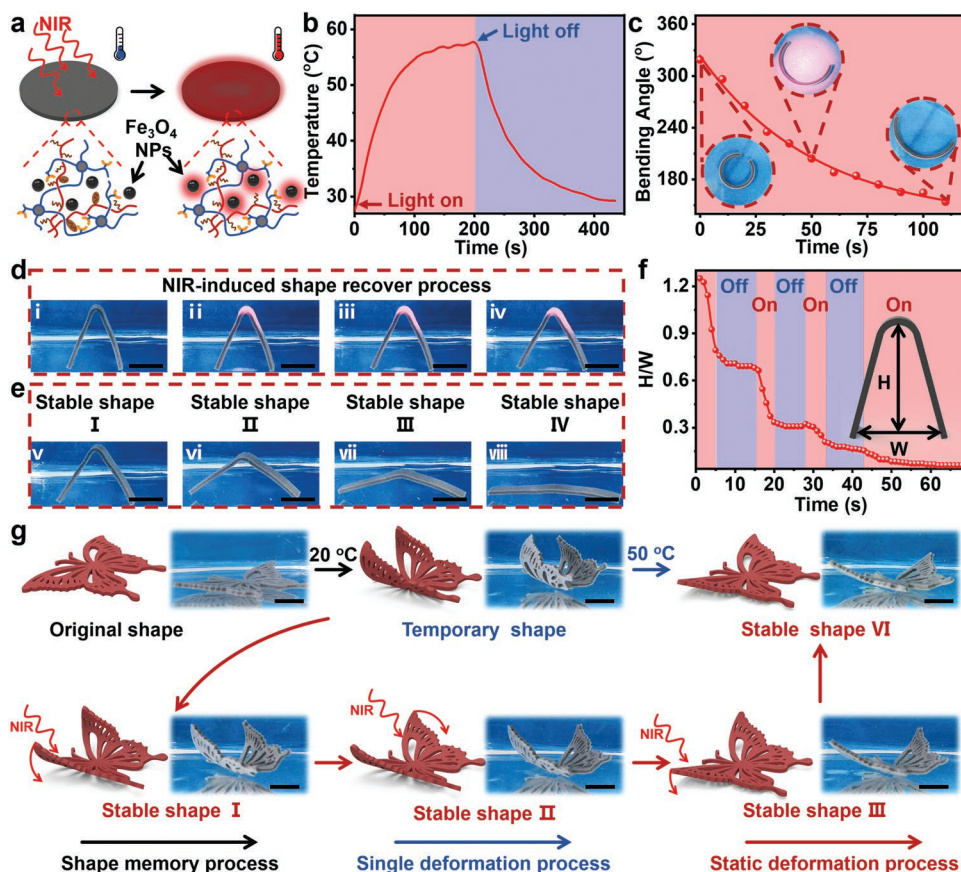
Figure 3. The static deformation process of PVA-C6 photothermal hydrogel under programmed NIR. a) Schematic illustration of the photothermal effect of PVA-C6 photothermal hydrogel contains of Fe_3O_4 NPs. b) The photothermal curve of PVA-C6 photothermal hydrogel. c) Variation of bending angles of the PVA-C6 photothermal hydrogel strip under NIR light. d) Images showing the NIR-induced shape recovery process of PVA-C6 photothermal hydrogel strip. e) Images showing the multi-stable shapes of PVA-C6 photothermal hydrogel strip during the deformation process. f) Quantitative analysis of the dynamic multi-stable shapes of PVA-C6 photothermal hydrogel strip during the deformation process. g) The multi-stable deformation process of butterfly-shaped PVA-C6 photothermal hydrogel. Scale bars : 1 cm.

shape to the target shape. Similarly, after a twice shape memory process, the PVA-C6 photothermal hydrogel could also exhibit continuous multi-stable deformation with the assistance of programmable NIR. For example, a hydrogel strip was bended into a circle and fixed the temporary shape in 50 °C Fe^{3+}, the hydrogel was flattened to the straight stripe again and fixed the temporary shape in 20 °C water. When the hydrogel strip was exposed to the NIR, it would self-deform from strip to circle owing to the photothermal effect of Fe_3O_4 NPs. During deformation process, when the strip deformed to the expected shape, the temporary shape could be quickly memorized by turning off the NIR. Therefore, the shape of the hydrogel strip could be precisely controlled according to the requirements (Figure S17 and Movie S6, Supporting Information). In addition, inspired by the origami, more complex encoded deformation could be occurred such as the transformation from the 2D hydrogel sheet to a 3D vase shape in the same way (Figure S18, Supporting Information).

Upon the exploration of the PVA-C6 photothermal hydrogel, we further propose a novel deformation mode, that is, a simple hydrogel strip that could provide multi-stable configurations after shape encoding once. Briefly, a hydrogel strip was folded

once and fixed the temporary shape in 50 °C Fe^{3+}. Then, the folded hydrogel is flattened to the straight stripe again and fixed the temporary shape in 20 °C water. Thus, the folded area is defined as a deformation node, n. If the hydrogel is only folded once, the value of n is 1. Subsequently, when the deformation node is slightly exposed under NIR, the hydrogel strip will slightly bulge and exhibit the stable shape I. Similarly, with the increase of the exposure time, the hydrogel strip will furtherly bulge to stable shape II and stable shape III, respectively. Therefore, the number of stable shapes, m, which is provided by a single deformation node, is 3 (**Figure 4**a). It is worth noting that a single deformation node could provide infinite stable shapes in theory, because every temporary shape within the deformation process could be fixed after removing the NIR. Furthermore, if there are n deformation nodes in a hydrogel strip, one deformation node could provide m stable shapes. So, a hydrogel strip would be able to generate m^n types of multi-stable shapes under the programmable irradiation of NIR (Figure 4b). For instance, a hydrogel strip was encoded with two deformation nodes in the same way as above. Then when the left deformation node was successively exposed under slight, moderate, and overdose NIR, the hydrogel strip would exhibit
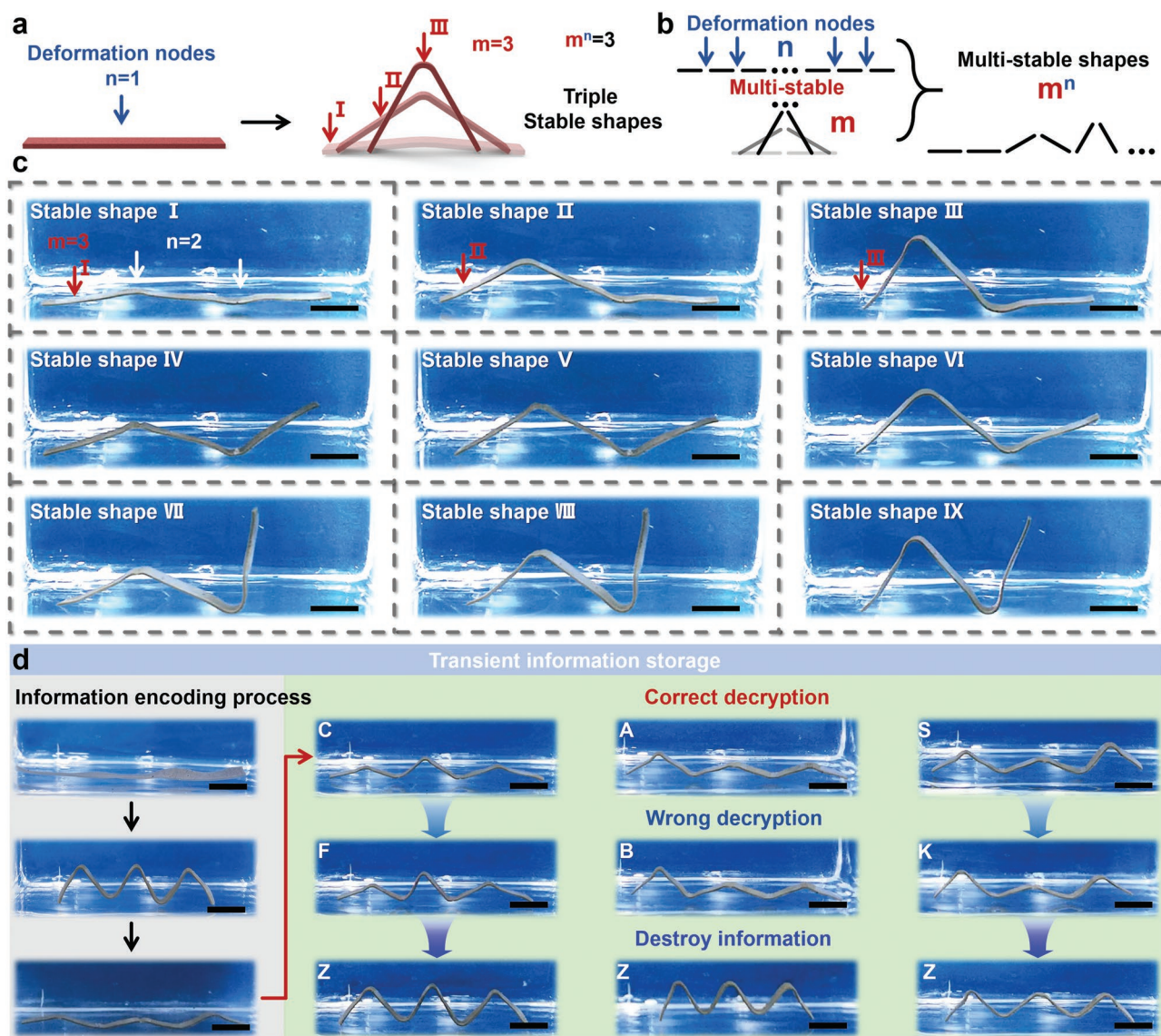
ADVANCED
SCIENCE NEWS
www.advancedsciencenews.com

ADVANCED
FUNCTIONAL
MATERIALS
www.afm-journal.de

Figure 4. The demonstration of transient information storage. a) Schematic illustration showing the triple stable shapes of PVA-C6 photothermal hydrogel strip with single deformation node ($n = 1$) and triple stable shape ($m = 3$). b) Schematic illustration showing the multi-stable shapes of PVA-C6 photothermal hydrogel strip. c) Images showing the nine types of configurations of PVA-C6 photothermal hydrogel strips when the number of deformation nodes is two and the number of stable shapes is three. d) Images showing the process of transient information storage. The PVA-C6 photothermal hydrogel strip was encoded with the configuration that represents the information of Z and fixed the temporary shape via ion-induced shape memory, then the hydrogel strip was flattened and fixed the temporary shape via thermo-induced shape memory. When the encoded hydrogel strip was correctly decrypted, the hydrogel strips would exhibit the correct configurations and express the right information. Scale bars : 1 cm.

stable shapes I, II, and III, respectively. Similarly, when the left deformation node was exposed under moderate NIR, while the right deformation node was successively exposed under slight, moderate, and overdose NIR, the hydrogel strip would provide stable shapes IV, V, and VI, respectively. Therefore, the hydrogel strip could provide a total of nine types of stable shapes under the programmable irradiation of NIR (Figure 4c).

Based on the discussion above, when the number of deformation nodes increases to five, and the stable shapes of a single deformation are three, the hydrogel strip could exhibit $3^5 = 243$ types of stable configurations. According to the diverse configurations, the hydrogel strip could be encoded with

all of the English letters including "space" and be applied for information encryption and decryption (Figure S19, Supporting Information). As shown in Figure 4d, a hydrogel strip with five deformation nodes was prepared first in the same way as above. If the hydrogel strip was decrypted by the correct process (irradiate the third deformation node with moderate NIR), the hydrogel strip would exhibit the correct configuration that represents the English letter "C". Similarly, irradiating the first deformation node with slight NIR, the hydrogel strip would exhibit the English letter "A". Besides, irradiating the first deformation node with moderate NIR and irradiating the fifth deformation node with overdose NIR, the hydrogel strip
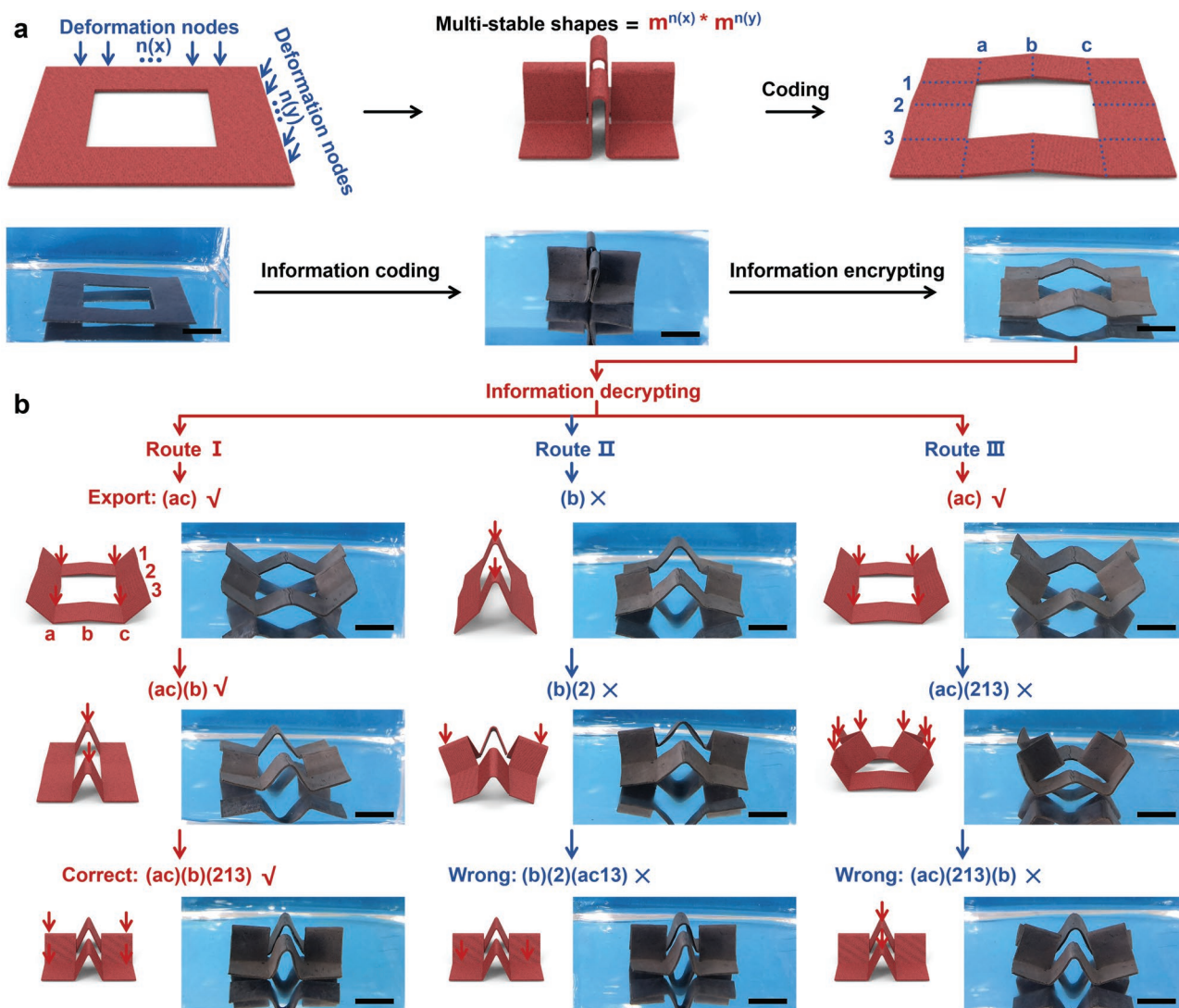
2206912 (8 of 12)

ADVANCED
SCIENCE NEWS
www.advancedsciencenews.com

ADVANCED
FUNCTIONAL
MATERIALS
www.afm-journal.de

Figure 5. The demonstration of hierarchical information encryption. a) Schematic illustration and images showing the 2D information encryption of hydrogel sheet via multi-stable deformation. b) Schematic illustration and images showing the stepwise decrypting process. The encrypted hydrogel could only exhibit the correct information when the correct encryption process is actuated. Scale bars: 1 cm.

would exhibit the English letter "S". Therefore, the complete information, CAS, which represents the "Chinese Academy of Sciences" was successfully decrypted. Unfortunately, if the wrong process was utilized, for example, the third deformation node was irradiated with overdoes NIR, the wrong information, "F", was exhibited. At last, after getting the right information, if the hydrogel strips were transferred to hot water, all of the hydrogel strips would deform to the initial shape which represents the English letter "Z", in order to destroy the information.

Furthermore, the 1D information encryption could be expanded to a higher level. As shown in **Figure 5**a, when the deformation nodes were introduced into both the *X*-axis and *Y*-axis of the hydrogel sheet, every axis of the hydrogel was able to generate m^n types of configurations as discussed above. Thus, a hydrogel sheet could exhibit $m^{n(x)} \times m^{n(y)}$ types of 3D configurations with the assistance of NIR, which furtherly motivated us to realize hierarchical information encryption. For

example, during the information coding process, the deformation nodes in the *X*-axis were encoded as a, b, and c successively while the *Y*-axis were encoded as 1, 2, and 3. In order to simplify the encryption process, the configuration generated by a single deformation node was limited to one. Thus, the hydrogel sheet would derive from nine types of 3D configuration. At this time, the encrypted information is not only the final configuration but also the deformation process. In other words, there were plenty of routes to reach the target shape but only one route is correct (Figure 5b). During the information decryption process, when the position a and c were irrited by NIR, the hydrogel sheet would deform to a "U" shape and export the corresponding result "(ac)". Then, when position b was irrited next, the shape of the hydrogel sheet would transfer from the "U" shape to the "Ω" shape, and simultaneously export the result "(ac)(b)". Finally, when positions 2, 1, and 3 were irrited, the 3D shape of the hydrogel sheet

would transfer again and export the encrypted information "(ac)(b)(213)". Interestingly, when the NIR wrongly irritated the position b first, then irritated position 2 and positions a, c, 1, 3, respectively, the final shape of the hydrogel sheet was the same, but the export result, "(b)(2)(ac13)", was wrong. Even if the NIR correctly irritated the position a and c first but it next wrongly irritated the position 2, 1, 3, and position b. Although, the final 3D shape is correct, the export result, "(ac)(213)(b)", was still wrong. Therefore, the correct information, digital code, was safely encrypted into various 3D shapes of the hydrogel sheet and the diverse deformation routes. Overall, the application of the PVA-C6 photothermal hydrogel in transient information storage hierarchical information encryption expands the applications of shape memory hydrogel.

3. Conclusion

In summary, in order to expand the information storage capacity of information encryption materials and improve the encryption level, a thermo and ion dual-responsive hydrogel containing thermo-mechanical PVA-C6 and ion-responsive P(AAm-co-AAc) polymer was fabricated, which was able to generate programmable deformation from the initial shape to the target shape via twice shape memory process and express the corresponding morphological information like gesture. Subsequently, with the incorporation of photothermal particle, Fe_3O_4, the PVA-C6 hydrogel would furtherly exhibit controllable and static deformability, which could suspend in any intermediate states and continuously transfer the corresponding morphological information.

With the introduction of the new concept (deformation node) into the hydrogel strip and sheet, we proposed two novel encryption modes: transient information storage and hierarchical information encryption. In order to decrypt the transient information, a user should get the correct key (the appropriate irradiation time and location) first, and the hydrogel strip could exhibit the correct configuration (the correct letter information). After decrypting the information, the configuration of the hydrogel strip would be reset by immersing in hot water. In hierarchical information encryption, the target information not only is encoded into the final shape of the hydrogel but also encoded into the deformation process. Only when the final shape and deformation process are all correct, can the user get the complete and correct information (digital code). We believe the information encryption based on programmable and static deformability will motivate the design and fabrication of shape deformation hydrogels, and expand the corresponding applications in the emerging field such as information encryption.

4. Experimental Section

Materials: Poly(vinyl alcohol) (PVA; M_w: 146000-186000), hexylamine, dimethyl sulfoxide (DMSO), acrylamide (AAm), acrylic acid (AAc), N,N'-methylene bis(acrylamide) (BIS), ammonium persulphate (APS), ferric chloride ($FeCl_3$), ethylene diamine tetraacetic acid (EDTA), 28% ammonia solution were purchased from Aladdin reagent Co. Ltd. N,N'-carbonyldiimidazole (CDI) purchased from Energy Chemical, China, and were used without further purification.

Instruments: The lyophilizing process was conducted in the DGJ-10C freeze dryer (Shanghai Boden Biological Science and Technology Co. Ltd.). The microstructure of the hydrogel was analyzed by field-emission scanning electron (Hitachi S-4800). The rheological measurements were performed on a stress-controlled rheometer (TA-dhr2) equipped with a geometry of 25 mm parallel plates in frequency sweep mode at room temperature.

The tensile tests were conducted on the Z1 Zwick/Roell Universal Testing System (Zwick). The photothermal performance was analyzed by a NIR laser source with a wavelength of 808 nm (BWT Beijing, K808DAHFN-15.00 W). The temperature was measured by an infrared camera (Opris PI-450i bought from Optris GmBH). The light transmittance of hydrogel was measured by virtue of TU-1810 UV–vis spectrophotometer provided by Purkinje General Instrument Co. Ltd. Tensile tests were performed at room temperature with the tensile speed of 10 mm min^{-1}. Samples were punched into dumbbell shapes (size: length × width × thickness: 50 mm × 3 mm × 1 mm).

Synthesis of PVA-C6: The PVA-C6 power was synthesized in accordance with the previous report [48] and the synthetic route was shown in Figure S3 (Supporting Information). In brief, poly(vinyl alcohol) (2 g, 45.5 mmol) was dissolved in 80 mL dry DMSO and heated to 90 °C for 3 h. When the solution was clarified, cooled down the temperature of the obtained solution to 20 °C. Then N,N'-carbonyldiimidazole (7.46 g, 45.5 mmol) was dissolved in the above solution with a magnetic stir bar for 3 h at 20 °C. Subsequently, 3 mL hexylamine (22.75 mmol) was slowly added to the CDI-activated PVA solution. The process usually lasted 15 min. After additional stirring for about 92 h, slowly added 3 mL 28% ammonia solution and kept stirring for 2 h. Then, the product, PVA-C6, was precipitated out in 800 mL of water. After filtering and repeatedly washing with water, the precipitate was collected. At last, PVA-C6 was obtained after freeze-drying.

Fabrication of PVA-C6 hydrogel and PVA-C6 Photothermal Hydrogel: 0.5 g PVA-C6 power was solved in 10 mL DMSO at 90 °C. After the temperature of the PVA-C6 solution cooled down to 20 °C, 1.4 mL AAc, 0.6 g AAm, 60 mg APS and 2 mg BIS were added and stirred to obtain a homogeneous solution. Then injected the solution into a home-make mold including one hollow silicone rubber sheet and two pieces of glass. The PVA-C6 hydrogel was obtained after polymerizing for 6 h at 60 °C and solvent exchange with water at 20 °C. The PVA-C6 photothermal hydrogel was fabricated similarly to PVA-C6 hydrogel except that the former needed to add 0.1 g Fe_3O_4 NPs to the hydrogel precursor.

Evaluation of Shape Memory Performance: The thermo-induced shape memory behaviors of PVA-C6 hydrogel were evaluated in water. A PVA-C6 hydrogel strip (size: length × width: 40 mm × 2 mm) was first bended into a circle in 50 °C water and then immersed into 20 °C water for a certain time to fix the temporary shape.

The ion-induced shape memory behaviors of PVA-C6 hydrogel were evaluated at 20 °C or 50 °C. A PVA-C6 hydrogel strip (size: length × width: 40 mm × 2 mm) was first bended into a circle and then immersed in 0.1 M $FeCl_3$ solution for a certain time to fix the temporary shape. All of the shape fixity ratios was defined by the following equation:

$$R_f = \theta_m / \theta_d \times 100\% \tag{1}$$

where the θ_m, θ_d are the bending angle of the memorized shape and hand-deformed shape of the hydrogel.

Evaluation of Dual-Responsive Shape Memory Performance: A PVA-C6 hydrogel strip (size: length × width: 40 mm × 2 mm) was first bended into a circle in 50 °C water and then immersed into 0.1 M 50 °C $FeCl_3$ solution for a certain time to fix the temporary shape I (R_{f1}). Subsequently, bended the circle into a straight stripe in 50 °C water, and immersed into 20 °C water for a certain time to fix the temporary II (R_{f2}). At last, the straight strip would recover to circle again when triggered in 50 °C water.

Evaluation of Photothermal Effect of PVA-C6 Photothermal Hydrogel: A PVA-C6 hydrogel sheet (size: length × width: 10 mm × 10 mm) was placed on the tin foil and irradiated by 5 W NIR (2 W cm^{-2}). The temperature was measured by an infrared camera.

**ADVANCED
SCIENCE NEWS**

www.advancedsciencenews.com

**ADVANCED
FUNCTIONAL
MATERIALS**

www.afm-journal.de

Measurement of the modification ratio of PVA-C6: As shown in Figure S4 (Supporting Information), the -OH group in the initial PVA was normalized to be one and presumed the modification ratio of hexylamine was X. Thus, the normalized number of protons from the terminal -CH_3 of hexylamine should be $3X$ while the normalized number of protons from the backbone of PVA and side hexyl-carbamate group should be $(2 \times 1 + 4 \times 2X)$. According to the ^1H NMR spectrum, the value of $(2 \times 1 + 4 \times 2X)/3X$ should be equated with the ratio between the integrated area of the characteristic peak of -CH_3 (chemical shift in 0.87) and -CH_2 (chemical shift from 4.59 to 5.73). Therefore, based on the equation $(2 \times 1 + 4 \times 2X)/3X = 12.41/3$, the X was solved as 0.45, which indicated the modification ratio of PVA-C6 was approximately ≈90%.

Statistical Analysis: All experiments were repeated at least three times. The error bars of experimental data were presented with mean ± standard deviation (SD). The size of the sample appeared in Figure 1b was 30 mm × 30 mm × 1 mm, Figure 1c was 40 mm × 5 mm × 1 mm, Figure 2c was 50 mm × 50 mm × 1 mm and 50 mm × 40 mm × 1 mm, Figure 3 was 40 mm × 5 mm × 1 mm and 40 mm × 35 mm × 1 mm, Figure 4 was 60 mm × 5 mm × 0.5 mm, Figure 5 was 40 mm × 40 mm × 0.5 mm. Images taken by mobile phones were processed by edge extraction, brightness, and contrast in the article. The software of Excel was employed to conduct a one-way analysis of variance (one-way ANOVA) and the difference among samples was considered to be important when the calculated p-value was <0.05.

Supporting Information

Supporting Information is available from the Wiley Online Library or from the author.

Acknowledgements

Conflict of Interest

The authors declare no conflict of interest.

Data Availability Statement

The data that support the findings of this study are available from the corresponding author upon reasonable request.

Keywords

[1] J. Heber, *Nat. Mater.* **2007**, *6*, 807.

[2] H. W. Zhang, Q. Y. Li, Y. B. Yang, X. F. Ji, J. L. Sessler, *J. Am. Chem. Soc.* **2021**, *143*, 18635.

[3] Y. C. Zhang, X. X. Le, Y. K. Jian, W. Lu, J. W. Zhang, T. Chen, *Adv. Funct. Mater.* **2019**, *29*, 1905514.

[4] Y. B. Yang, Q. Y. Li, H. W. Zhang, H. Liu, X. F. Ji, B. Z. Tang, *Adv. Mater.* **2021**, *33*, 2105418.

[5] C. Y. Zhang, B. Wang, W. B. Li, S. Q. Huang, L. Kong, Z. C. Li, L. Li, *Nat. Commun.* **2017**, *8*, 1138.

[6] X. X. Le, H. Shang, S. S. Wu, J. W. Zhang, M. J. Liu, Y. F. Zheng, T. Chen, *Adv. Funct. Mater.* **2021**, *31*, 2108365.

[7] Y. Sun, X. Le, S. Zhou, T. Chen, *Adv. Mater.* **2022**, *34*, 2201262.

[8] Z. Q. Li, H. Z. Chen, B. Li, Y. M. Xie, X. L. Gong, X. Liu, H. R. Li, Y. L. Zhao, *Adv. Sci.* **2019**, *6*, 1901529.

[9] C. N. Zhu, T. W. Bai, H. Wang, J. Ling, F. H. Huang, W. Hong, Q. Zheng, Z. L. Wu, *Adv. Mater.* **2021**, *33*, 2102023.

[10] Y. Qi, W. B. Niu, S. F. Zhang, S. L. Wu, L. Chu, W. Ma, B. T. Tang, *Adv. Funct. Mater.* **2019**, *29*, 1906799.

[11] P. Li, D. Zhang, Y. C. Zhang, W. Lu, J. W. Zhang, W. Q. Wang, Q. S. He, P. Théato, T. Chen, *ACS Macro Lett.* **2019**, *8*, 937.

[12] Y. Su, S. Z. F. Phua, Y. Li, X. J. Zhou, D. Jana, G. F. Liu, W. Q. Lim, W. K. Ong, C. L. Yang, Y. L. Zhao, *Sci. Adv.* **2018**, *4*, eaas9732.

[13] X. X. Le, H. Shang, H. Z. Yan, J. W. Zhang, W. Lu, M. J. Liu, L. P. Wang, G. M. Lu, Q. J. Xue, T. Chen, *Angew. Chem., Int. Ed.* **2020**, *59*, 2.

[14] B. Y. Wu, H. H. Lu, X. X. Le, W. Lu, J. W. Zhang, P. Théato, T. Chen, *Chem. Sci.* **2021**, *12*, 6472.

[15] R. Kempaiah, Z. H. Nie, *J. Mater. Chem. B* **2014**, *2*, 2357.

[16] J. J. Shang, X. X. Le, J. W. Zhang, T. Chen, P. Théato, *Polym. Chem.* **2019**, *10*, 1036.

[17] W. Lu, X. X. Le, J. W. Zhang, Y. J. Huang, T. Chen, *Chem. Soc. Rev.* **2017**, *46*, 1284.

[18] C. Lowenberg, M. Balk, C. Wischke, M. Behl, A. Lendlein, *Acc. Chem. Res.* **2017**, *50*, 723.

[19] Y. L. Xia, Y. He, F. H. Zhang, Y. J. Liu, J. S. Leng, *Adv. Mater.* **2020**, *33*, 2000713.

[20] W. Yuan, C. Yu, S. Xu, L. Ni, W. Xu, G. Shan, Y. Bao, P. Pan, *Mater. Horiz.* **2022**, *9*, 756.

[21] X. X. Le, W. Lu, J. He, M. J. Serpe, J. W. Zhang, T. Chen, *Sci. China Mater.* **2018**, *62*, 831.

[22] S. T. Wang, M. J. Liu, L. Gao, G. Q. Guo, Y. P. Huo, *ACS Appl. Mater. Interfaces* **2019**, *11*, 19554.

[23] C. F. Dai, C. Du, Y. Xue, X. N. Zhang, S. Y. Zheng, K. Liu, Z. L. Wu, Q. Zheng, *ACS Appl. Mater. Interfaces* **2019**, *11*, 43631.

[24] Z. G. Zhao, S. Y. Zhuo, R. C. Fang, L. H. Zhang, X. T. Zhou, Y. C. Xu, J. Q. Zhang, Z. C. Dong, L. Jiang, M. J. Liu, *Adv. Mater.* **2018**, *30*, 1804435.

[25] W. J. Peng, G. G. Zhang, J. Liu, S. Nie, Y. Wu, S. H. Deng, G. Q. Fang, J. Zhou, J. Z. Song, J. Qian, P. J. Pan, Q. Zhao, T. Xie, *Adv. Funct. Mater.* **2020**, *30*, 2000522.

[26] X. X. Le, W. Lu, J. W. Zhang, T. Chen, *Adv. Sci.* **2019**, *6*, 1801584.

[27] C. Ni, D. Chen, Y. Zhang, T. Xie, Q. Zhao, *Chem. Mater.* **2021**, *33*, 2046.

[28] W. X. Fan, C. Y. Shan, H. Y. Guo, J. W. Sang, R. Wang, R. R. Zheng, K. Y. Sui, Z. H. Nie, *Sci. Adv.* **2019**, *5*, eaav7174.

[29] X. P. Hao, Z. Xu, C. Y. Li, W. Hong, Q. Zheng, Z. L. Wu, *Adv. Mater.* **2020**, *32*, 2000781.

[30] X. L. Gong, Y. Y. Xiao, M. Pan, Y. Kang, B. J. Li, S. Zhang, *ACS Appl. Mater. Interfaces* **2016**, *8*, 27432.

[31] H. L. Cui, N. Pan, W. X. Fan, C. Z. Liu, Y. Y. Li, Y. Z. Xia, K. Y. Sui, *Adv. Funct. Mater.* **2019**, *29*, 1807692.

[32] C. Y. Li, X. P. Hao, S. Y. Zheng, W. Hong, Q. Zheng, Z. L. Wu, *Adv. Intell. Syst.* **2019**, *1*, 1900055.

[33] Z. G. Zhao, Y. X. Liu, K. J. Zhang, S. Y. Zhuo, R. C. Fang, J. Q. Zhang, L. Jiang, M. J. Liu, *Angew. Chem., Int. Ed.* **2017**, *56*, 13464.

**ADVANCED
SCIENCE NEWS**

www.advancedsciencenews.com

**ADVANCED
FUNCTIONAL
MATERIALS**

www.afm-journal.de

[34] Q. J. Ze, X. Kuang, S. Wu, J. Wong, S. M. Montgomery, R. D. Zhang, J. M. Kovitz, F. Y. Yang, H. J. Qi, R. K. Zhao, *Adv. Mater.* **2020**, *32*, 1906657.

[35] Q. Zhang, X. Kuang, S. Y. Weng, L. Yue, D. J. Roach, D. N. Fang, H. J. Qi, *Adv. Funct. Mater.* **2021**, *31*, 2010872.

[36] Y. Zhang, X. Y. Yin, M. Y. Zheng, C. Moorlag, J. Yang, Z. L. Wang, *J. Mater. Chem. A* **2019**, *7*, 6972.

[37] L. Cera, G. M. Gonzalez, Q. H. Liu, S. J. Choi, C. O. Chantre, J. Lee, R. Gabardi, M. C. Choi, K. Shin, K. K. Parker, *Nat. Mater.* **2020**, *20*, 242.

[38] Z. J. Ding, L. Yuan, G. Z. Liang, A. J. Gu, *J. Mater. Chem. A* **2019**, *7*, 9736.

[39] R. X. Liang, H. J. Yu, L. Wang, N. Wang, B. U. Amin, *Adv. Funct. Mater.* **2021**, *31*, 2102621.

[40] B. Zhang, H. G. Li, J. X. Cheng, H. T. Ye, A. H. Sakhaei, C. Yuan, P. Rao, Y. F. Zhang, Z. C. Chen, R. Wang, X. N. He, J. Liu, R. Xiao, S. X. Qu, Q. Ge, *Adv. Mater.* **2021**, *33*, 2101298.

[41] X. B. Hu, D. X. Zhang, S. S. Sheiko, *Adv. Mater.* **2018**, *30*, 1707461.

[42] Y. K. Jian, X. X. Le, Y. C. Zhang, W. Lu, L. Wang, J. Zheng, J. W. Zhang, Y. J. Huang, T. Chen, *Macromol. Rapid. Commun.* **2018**, *39*, 1800130.

[43] W. Lu, C. X. Ma, D. Zhang, X. X. Le, J. W. Zhang, Y. J. Huang, C. F. Huang, T. Chen, *J. Phys. Chem. C* **2018**, *122*, 9499.

[44] Y. C. Zhang, X. X. Le, W. Lu, Y. K. Jian, J. W. Zhang, T. Chen, *Macromol. Mater. Eng.* **2018**, *303*, 1800144.

[45] Y. C. Zhang, Q. Q. Hu, S. R. Yang, T. Wang, W. X. Sun, Z. Tong, *Macromolecules* **2021**, *54*, 5218.

[46] H. Xiao, W. Lu, X. X. Le, C. X. Ma, Z. W. Li, J. Zheng, J. W. Zhang, Y. J. Huang, T. Chen, *Chem. Commun.* **2016**, *52*, 13292.

[47] X. X. Le, W. Lu, H. Xiao, L. Wang, C. X. Ma, J. W. Zhang, Y. J. Huang, T. Chen, *ACS Appl. Mater. Interfaces* **2017**, *9*, 9038.

[48] S. T. Wang, S. J. Li, L. Gao, *ACS Appl. Mater. Interfaces* **2019**, *11*, 43622.

2206912 (12 of 12)